Morphology Formation by Combined Effect of Crystallization and Phase Separation in a Binary Blend of Poly(ϵ-caprolactone) and Polystyrene Oligomer

Shuichi Nojima,* Kunihiko Satoh, and Tamaichi Ashida

Department of Applied Chemistry, Nagoya University, Nagoya 464-01, Japan

Received June 25, 1990; Revised Manuscript Received August 10, 1990

ABSTRACT: The morphology, formed as a combined effect of crystallization and liquid–liquid phase separation in a binary blend of poly(ϵ-caprolactone) (PCL) and polystyrene oligomer (PSO) at various crystallization temperatures and compositions, is investigated by means of small-angle X-ray scattering (SAXS). This PCL–PSO system shows an UCST-type phase separation. The observed shape of the SAXS curve and the angular position of the intensity peak varied significantly with the PCL composition in the blend, but slightly with the crystallization temperature. Parameters characterizing the morphology, such as lamellar thickness and amorphous layer thickness, are evaluated by employing the Hosemann–Tsvankin model and the Vonk–Kortleve model. These results can be successfully explained in terms of the phase diagram consisting of the binodals and melting points of PCL.

Introduction

Crystallization and liquid–liquid phase separation are dominant factors to produce the morphology in polymer blend systems.[1] The systems usually used for the study of phase separation are blends of noncrystalline polymers in order to exclude the morphology based on the crystallization of constituent polymers.[2,3] In the morphological studies by crystallization, on the other hand, compatible blend systems over the whole composition range are used to avoid morphology formation owing to the phase separation between components.[4] In practical cases, in which the blend systems are made up of more than two components, crystallization will take place simultaneously with phase separation over the temperature range we are interested in. The phase diagram for polymer blends exhibiting both crystallization and phase separation has been theoretically predicted.[5-7] Burghardt,[7] for example, calculated the phase diagram of such systems on the basis of the Flory–Huggins theory. Morphological control by these two phase transitions was also performed in a polypropylene/ethylene–propylene copolymer system by Hashimoto et al.[8,9] Thus, two kinds of phase transition may introduce an additional complexity to the morphology of such polymer blend systems. Another example of the competition of two phase transitions is the combination of macro- and microphase separations recently studied theoretically[10] and experimentally[11,12] for a block copolymer–homopolymer system. In these studies, complicated morphology due to the cooperation of two phase transitions is also predicted. The phase diagram of such a system is not merely the sum of the contributions from the two phase transitions, and additional features appear in it.[12]

We have recently investigated the morphology produced in a binary blend of poly(ϵ-caprolactone) (PCL) and polystyrene oligomer (PSO) at various PCL compositions (ϕ_{PCL}) by small-angle X-ray scattering (SAXS) when PCL crystallized at room temperature (25 °C).[13] This system has an UCST-type coexistence curve with the critical composition about $\phi_{PCL} = 0.2$, and PCL crystallizes below 60 °C in the blend. The crystallization of PCL in the blend was accompanied by the phase separation even for the blend quenched into the region outside the coexistence curve, and consequently a complicated morphology was built up, which was intimately dependent on ϕ_{PCL}. Tanaka and Nishi[14,15] observed spherulite growth in a PCL–PSO blend by optical microscopy, and showed that at a high crystallization temperature (~50 °C), the PSO-rich phase came out from the spherulite to make a macroscopic phase on the boundary of the spherulite, while at a low temperature (~35 °C), the PSO-rich phase remained within the spherulite to make the microscopic picture of the spherulite complicated.

In the present study, the morphology of a PCL–PSO system with various PCL compositions is investigated by means of SAXS when PCL crystallizes at various temperatures spanning from room temperature to 45 °C. The parameters characterizing the morphology, such as lamellar thickness and amorphous layer thickness, are evaluated by employing the Hosemann–Tsvankin model[16] and the Vonk–Kortlevel model.[17] The bulk crystallinity of the blend is independently measured by differential scanning calorimetry (DSC). The dependence of such parameters on the crystallization temperature and PCL composition is discussed on the basis of the phase diagram of this system.

Experimental Section

1. Materials and Sample Preparation. The poly(ϵ-caprolactone) (PCL) used in this study was supplied by Scientific Polymer Products Inc. and was fractionated with a benzene–methanol system. The weight-average molecular weight M_w was 13 700, and the ratio of M_w to number-average molecular weight M_n, M_w/M_n, determined by gel permeation chromatography was 1.44. Polystyrene oligomer (PSO) was purchased from Tosoh Corp., and M_w and M_w/M_n were stated to be 950 and 1.13, respectively.

The solvent-casting method was employed to prepare blends with various ϕ_{PCL} ranging from 0.55 to 1. PCL and PSO were dissolved in a common solvent, benzene, at a polymer concentration less than 15%. The solution was cast on a glass plate, and the solvent was evaporated under vacuum at 80 °C for more than 40 h. The blends thus prepared were kept until use at a temperature above the melting temperature of PCL ($T_m \sim 60$ °C) to prevent crystallization of PCL.

2. Differential Scanning Calorimetry (DSC) Measurement. A Perkin-Elmer Model 4 DSC was used to determine the melting temperature of PCL and the crystallinity of the blend. The sample, first annealed at 100 °C for 1–2 h, was crystallized by quenching at the maximum rate (−500 °C/min) to the crystallization temperature T_c ranging from 25 to 45 °C, followed by heating at a rate of 10 °C/min. The quench process was completely finished before PCL started to crystallize. The crystallinity and the melting temperature of PCL in the blend

0024-9297/91/2224-0942$02.50/0

were evaluated from the peak area and peak position of the endothermic curve. The exothermic heat flow during crystallization was also monitored to ensure the end of crystallization at each T_c.

3. Small-Angle X-ray Scattering (SAXS) Measurement. SAXS measurement was performed with an Anton Paar small-angle camera equipped with a Kratky collimation system and a step-scanning scintillation counter.[13] The radiation used was Cu Kα (λ = 1.542 Å) monochromatized by a Ni filter. The entrance and counter slits were 100 and 75 μm in width, and the distance between the sample and the plane of registration was 21.7 cm. The X-ray intensity scattered from each blend was measured after the blend was quenched from the melt and completely crystallized in the sample cell of the SAXS apparatus at temperatures between 25 and 45 °C. The time necessary for each measurement was ca. 12 h, during which the sample was kept at each T_c within the fluctuation of 0.5 °C.

The correction for the slit-width and slit-length smearing was made by Glatter's algorithm[18] to obtain the desmeared intensity I_{des}. The background intensity I_{back}, which represents the deviation from Porod's law,[19], was estimated by the relation

$$I_{des}(s) = As^{-4} + I_{back} \tag{1}$$

in an intermediate range of s, where A is a constant and $s = 2 \sin \theta/\lambda$, 2θ being the scattering angle. After extrapolating the corrected intensity to smaller and larger angles by Guinier's and Porod's laws, respectively, the one-dimensional correlation function $\gamma(x)$ was evaluated by the relation

$$\gamma(x) = \frac{\int_0^\infty s^2 I_{des} \cos(2\pi x s)\, ds}{\int_0^\infty s^2 I_{des}\, ds} \tag{2}$$

4. Analysis of SAXS Curve. The SAXS curve obtained was analyzed by means of two models: (1) the Hosemann-Tsvankin model (H-T model)[16] and (2) the Vonk-Kortleve model (V-K model).[17] In the H-T model, which is based on a paracrystalline model, each crystalline domain consists of N alternating stacks of lamella and amorphous layer. The one-dimensional scattered intensity $i(s)$ ($\propto s^2 I_{des}$) calculated from this model is given by

$$i(s) = \left\{ \mathrm{Re}\left(N \frac{(1-f_c)(1-f_a)}{1-f_c f_a} \right) + \mathrm{Re}\left[f_a \left(\frac{1-f_c}{1-f_c f_a} \right)^2 [1 - (f_c f_a)^N] \right] \right\} Z(s)/(2\pi^2 s^2) \tag{3}$$

where $Z(s)$ represents the profile of the transition layer between the lamella and amorphous layer,[20] N is the mean number of the repeating unit of the lamella and amorphous layer within a crystalline domain, and f_c and f_a are the Fourier transforms of the thickness distribution functions $h_c(x)$ and $h_a(x)$ of the lamella (with mean thickness l_c) and amorphous layer (l_a) given by

$$h_c(x) = \frac{1}{\beta_c (2\pi)^{1/2}} \exp\left(-\frac{(x-l_c)^2}{2\beta_c^2} \right) \tag{4}$$

$$h_a(x) = \frac{1}{\beta_a (2\pi)^{1/2}} \exp\left(-\frac{(x-l_a)^2}{2\beta_a^2} \right) \tag{5}$$

Equation 3 was fitted with the experimentally observed $s^2 I_{des}(s)$, and the parameters included in the model were evaluated as a function of both ϕ_{PCL} and T_c. The fit was achieved by the Gauss-Newton algorithm. The estimation of the best values of the parameters, l_c, l_a, and N was relatively easy, and their values were not much affected when a fairly wide latitude was given to the choice of other parameters. In contrast, meaningful values of the parameters β_c and β_a were difficult to evaluate, and therefore no attempt has been made to interpret them.

The Kortleve-Vonk model is characterized by the infinite number of alternately repeating units of the lamellae and amorphous layers. The one-dimensional correlation function derived from this model is expressed as

$$\gamma(x) = \frac{\chi_c}{1-\chi_c}\left(\frac{1}{\chi_c^2} \int_0^\infty (x_c - x) h_c(x_c)\, dx_c + P_{cac} + P_{cacac} + \ldots - 1 \right) \tag{6}$$

where χ_c is the linear crystallinity defined as $\chi_c = l_c/(l_c + l_a)$ and the terms $P_{ca\ldots c}$ indicate convolution products of the type $q_c h_a h_c \ldots q_c$ in which

$$q_c(x) = \int_x^\infty h_c(x_c)/\chi_c\, dx_c \tag{7}$$

Four parameters, l_c, l_a, β_c, and β_a, were determined by curve fitting with the information about the long period L ($=l_c + l_a$) determined from the first maximum of the experimental correlation function. Two parameters, l_c and l_a, were sensitive to the shape of the correlation function experimentally obtained and therefore can be easily determined.

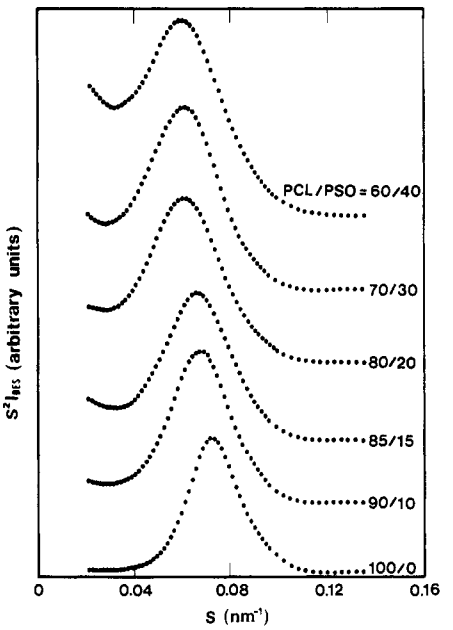

Figure 1. Lorentz-corrected X-ray intensities, scattered from blends crystallized at 33 °C containing 100, 90, 85, 80, 70, and 60% poly(ϵ-caprolactone), are plotted against s ($=2 \sin \theta/\lambda$). The plots for data with PCL/PSO = 90/10, 85/15, 80/20, 70/30, and 60/40 are shifted upward successively for legibility.

Results

1. Scattering Curves. The phase diagram of the PCL-PSO system, the cloud point curve and melting points of PCL, is shown in Figure 1 of our previous paper.[13] This system has an UCST-type coexistence curve with the critical composition in the vicinity of $\phi_{PCL} = 0.2$. The melting temperature of PCL in the blend decreases steadily with decreasing ϕ_{PCL} and intersects with the cloud point curve at about $\phi_{PCL} = 0.5$.

Figure 1 shows the Lorentz-corrected X-ray intensity scattered from various blends crystallized at T_c = 33 °C, where the abscissa is the wavenumber $s = 2 \sin \theta/\lambda$ with 2θ being scattering angle. The angular position of the intensity peak, which is ca. 0.07 nm^{-1} for pure PCL ($\phi_{PCL} = 1$), shifts toward smaller s with decreasing ϕ_{PCL} and is invariable ($s \sim 0.06$ nm^{-1}) for the blends with $\phi_{PCL} \leq 0.7$. Another characteristic feature of Figure 1 is the appearance of the scattered intensity at smaller s, which is insignificant for $\phi_{PCL} > 0.85$ and hence not detectable, but becomes more significant with decreasing ϕ_{PCL}. The SAXS intensity for $\phi_{PCL} \leq 0.85$ looks like the superposition of the two scattered intensities, one having a peak at $s \sim 0.06$ nm^{-1} and arising from the crystalline domain which consists

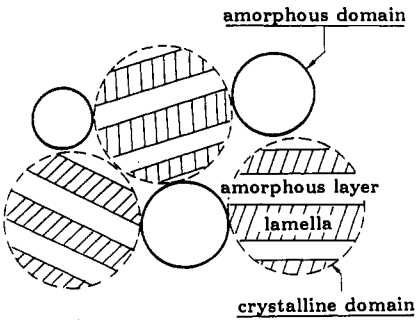

Figure 2. Schematic illustration of the two-phase structure based on the one-dimensional model of Hosemann. The size and proportion of the amorphous domain will change significantly with PCL composition ϕ_{PCL} and crystallization temperature T_c. The lamella and amorphous layer repeat alternately within the crystalline domain.

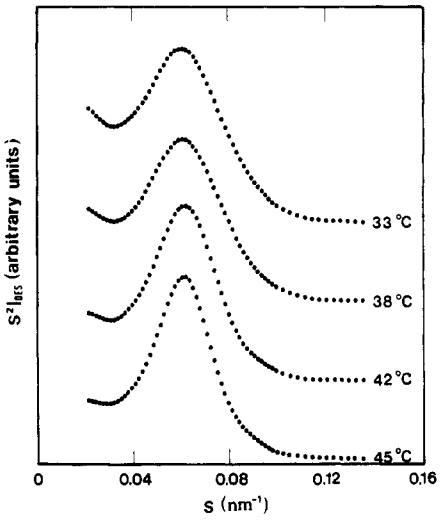

Figure 3. Lorentz-corrected X-ray intensities, scattered from the blend containing 55% PCL and crystallized at 33, 38, 42, and 45 °C, are plotted against s.

of the alternating stacks of the lamella and amorphous layer, and another increasing intensity as $s \to 0$, suggesting its peak is probably located at $s = 0$. In our previous study,[13] the second component of the scattered intensity was attributed to the two-phase structure of the system consisting of the crystalline domain (with the lamella and amorphous layer) and amorphous domain. At pure PCL, the system is a mosaic structure of the crystalline domains. As the PSO component increases, the amorphous domain appears among crystalline domains (Figure 2), and eventually the amorhpous domains develop into a matrix phase by connecting to each other. The average electron-density difference between two domains makes the scattered intensity at lower angles. The amorphous domain is rich in PSO and is produced by the combined effect of the crystallization and liquid–liquid phase separation when PCL crystallizes in the blend. The mechanism for the formation of this amorphous domain will be discussed later.

Figure 3 shows the Lorentz-corrected intensities for the blend with $\phi_{PCL} = 0.55$ crystallized at the various temperatures indicated. The angular position of the peak is ca. 0.06 nm^{-1} for all T_c, while the second component of the scattered intensity appearing at smaller s decreases in magnitude with increasing T_c compared to the first component scattered from the crystalline domain. This decrease could be observed for all samples that have a pronounced second component of the scattered intensity. The intensity change with T_c observed in Figure 3 is probably explained by two factors: (1) composition change

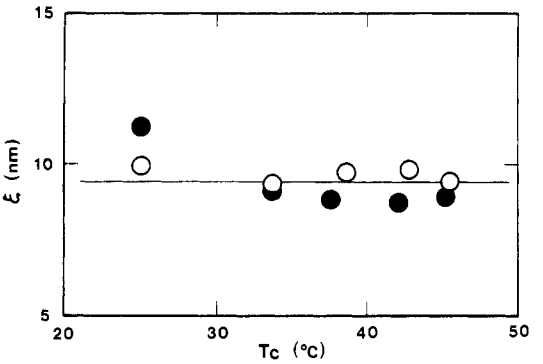

Figure 4. Correlation length ξ, evaluated from the Debye–Bueche relation, is plotted against crystallization temperature T_c: (○) PCL/PSO = 70/30; (●) 55/45.

of the amorphous domain and of the amorphous layer between lamellae within the crystalline domain during the course of crystallization, which will be discussed later, and (2) temperature dependence of the thermal expansion coefficient, which is generally larger for the liquid state than for the solid state. That is, the electron-density contrast between two domains (crystalline and amorphous domains), which yields the SAXS intensity at smaller s, is strongly dependent on the temperature compared to that between the lamella and amorphous layer within a crystalline domain.

2. Analysis with the Hosemann–Tsvankin Model. For blends containing a large amount of PSO (smaller ϕ_{PCL}), the curve fitting with the theoretical intensity (eq 3) becomes impractical because of the presence of the extraneous component of the scattered intensity at smaller s, as shown in Figures 1 and 3. This scattered intensity was assumed in our previous paper[13] to arise from the two-phase structure with the crystalline and amorphous domains (Figure 2) and was approximated by the Debye–Bueche relation,[21] which is generally applicable and widely used for the scattered intensity from the two-phase structure on the assumption that the X-ray intensity scattered from the crystalline domain is negligibly small at smaller s

$$I_{des}(s) = \frac{K\langle(\rho_1 - \rho_2)^2\rangle\xi^3}{(1 + 4\pi^2 s^2 \xi^2)^2} \tag{8}$$

where ρ_1 and ρ_2 are the electron densities of phases 1 and 2, ξ is the correlation length of the electron-density fluctuation, and K is a constant. The equation can be rewritten as

$$\frac{1}{[I_{des}(s)]^{1/2}} = \frac{4\pi^2\xi^2 s^2}{[K\langle(\rho_1 - \rho_2)^2\rangle\xi^3]^{1/2}} + \frac{1}{[K\langle(\rho_1 - \rho_2)^2\rangle\xi^3]^{1/2}} \tag{9}$$

Therefore, the plot of $1/[I_{des}(s)]^{1/2}$ against s^2 should be linear at smaller s. An example of such a plot is shown in Figure 5 of our previous paper.[13] Every SAXS curve that has the pronounced second component of the scattered intensity shows a straight line at smaller s, and the estimation of the best values of the parameters ξ and $K\langle(\rho_1 - \rho_2)^2\rangle$ was relatively easy from the slope and intercept of the line. The plot of ξ thus evaluated is shown in Figure 4 as a function of T_c, where ξ is ca. 9.5 nm irrespective of T_c and ϕ_{PCL}, though the data points are somewhat scattered. This ξ value is larger than l_c and l_a (described below), suggesting that the blend has another superstructure in addition to the repeating structure of the lamella and amorphous layer within a crystalline domain.

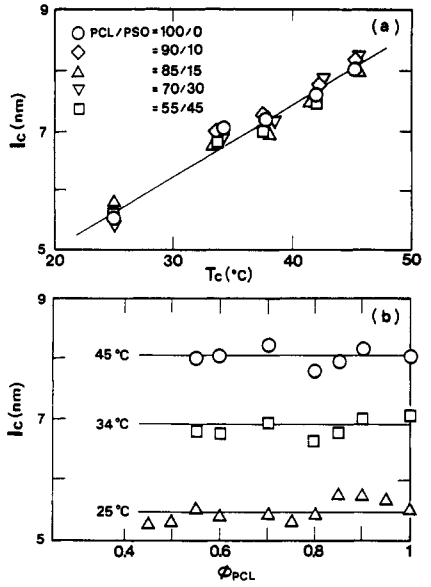

Figure 5. Lamellar thickness l_c, evaluated through the curve fitting with the theoretical intensity based on the Hosemann–Tsvankin model, is plotted against T_c (a) and ϕ_{PCL} (b).

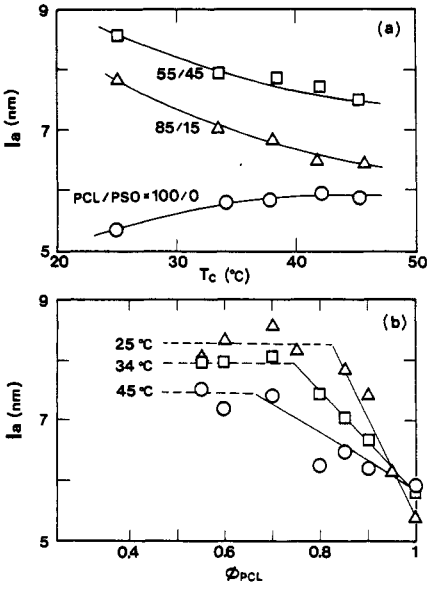

Figure 6. Amorphous layer thickness l_a, evaluated through the same procedure as described in Figure 5, is plotted against T_c (a) and ϕ_{PCL} (b).

The l_c and l_a, evaluated by employing the Hosemann–Tsvankin model (H–T model), are plotted in Figures 5 and 6. Figure 5a shows the T_c dependence of l_c and Figure 5b the ϕ_{PCL} dependence of l_c, where l_c increases linearly with T_c, while it is invariable against ϕ_{PCL}. Figure 5 suggests that the size of the PCL lamella formed in the blend is significantly affected by the crystallization temperature but not by the existence of the amorphous component, PSO, in the system. Figure 6 shows the T_c and ϕ_{PCL} dependence of l_a, where l_a changes smoothly with T_c, while it shows a complicated change against ϕ_{PCL}; l_a increases linearly as ϕ_{PCL} deviates from 1, with the slope being larger as T_c decreases, and levels off over the intermediate range of ϕ_{PCL}. This variation of l_a reflects the ϕ_{PCL} dependence of the peak position of the SAXS intensity shown in Figure 1 and was previously interpreted by the combined effect of the crystallization and liquid–liquid phase separation during the process of morphology formation in the system.[13] When PCL crystallizes in the blend, the amorphous component, PSO, is rejected from

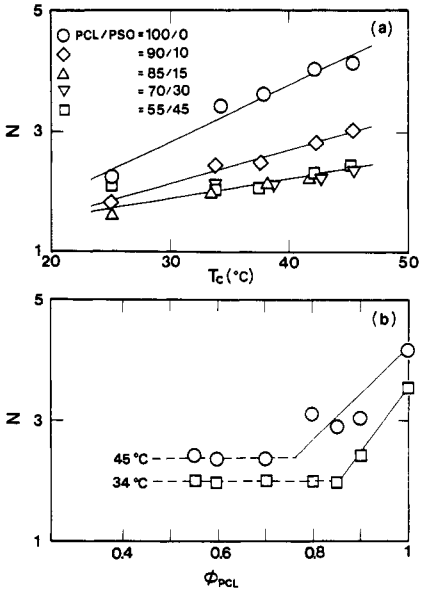

Figure 7. Average number N of the repeating unit of the lamella and amorphous layer within a crystalline domain is plotted against T_c (a) and ϕ_{PCL} (b).

the lamellae to be accommodated in the amorphous layer between lamellae. This PSO makes l_a larger with decreasing ϕ_{PCL}. For further decrease of ϕ_{PCL}, liquid–liquid phase separation takes place in the amorphous layer to make another new domain which is rich in PSO. The difference in the average electron density between the new domain and the crystalline domain (consisting of the lamella and amorphous layer) brings about the increasing SAXS intensity at smaller s. When the phase diagram of this PCL–PSO system is taken into account, the mechanism of this morphology formation may be slightly modified. The details will be mentioned in the Discussion.

Figure 7 shows the T_c and ϕ_{PCL} dependence of N, where N represents the average number of alternating units of lamellae and amorphous layers when they are approximated to be perfectly arranged within a crystalline domain. The value of N increases with T_c, suggesting that the packing of the lamellae within a crystalline domain, and thus the crystallinity within the domain, becomes more perfect with increasing T_c. The ϕ_{PCL} dependence of N can be interpreted in terms of the ϕ_{PCL} dependence of l_a. N decreases linearly as ϕ_{PCL} deviates from 1, which reflects the distortion of the repeating unit of the lamella and amorphous layer because of the intervention of PSO in the amorphous layer. Further decrease of ϕ_{PCL} results in a constancy of N, in agreement with the fact that the characteristic sizes within a crystalline domain, such as the lamellar thickness and amorphous layer thickness, do not change with the decrease of ϕ_{PCL}.

3. Analysis with the Vonk–Kortleve Model. Figure 8 shows the T_c dependence of l_c evaluated on the basis of the Vonk–Kortleve model (V–K model). This l_c increases certainly with increasing T_c and is invariable against ϕ_{PCL}, though the data points are somewhat scattered. Figure 9 shows the ϕ_{PCL} dependence of l_a, where the variation of l_a against ϕ_{PCL} is the same as that in Figure 6b; first l_a increases with decreasing ϕ_{PCL} and then it levels off at intermediate ϕ_{PCL}. The T_c dependence of l_a cannot be clearly observed in Figure 9. The V–K model includes four parameters, l_c, l_a, β_c, and β_a, to be adjusted, in which only l_c and l_a affect so much the shape and maximum position of the correlation function. This means that a small change in the shape of the experimental correlation function, which may happen during the SAXS measure-

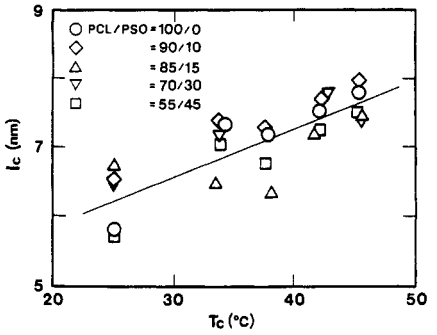

Figure 8. l_c, evaluated through the curve fitting with the theoretical correlation function based on the Vonk–Kortleve model, is plotted against T_c.

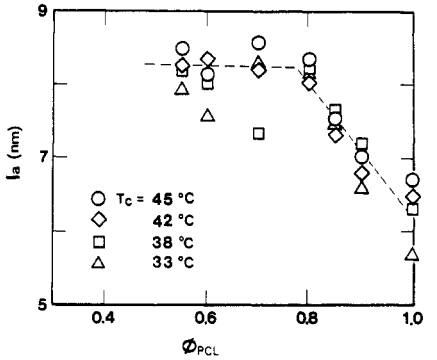

Figure 9. l_a, evaluated through the same procedure as described in Figure 8, is plotted against ϕ_{PCL}.

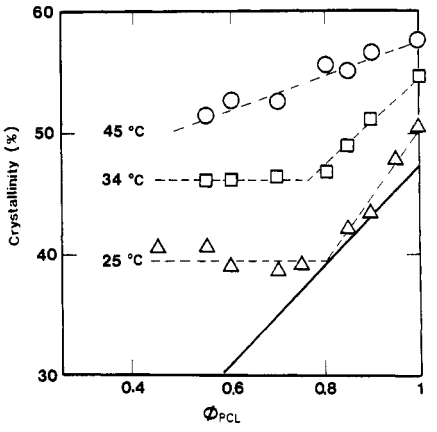

Figure 10. Linear crytallinity χ, evaluated through the curve fitting with the theoretical intensity based on the Hosemann–Tsvankin model, is plotted against ϕ_{PCL}. The solid line represents the bulk crystallinity χ' measured by DSC. The T_c dependence of χ' is negligibly small.

ment and data processing, seriously affects the final values of l_c and l_a and therefore leads to scattering of the data points.

4. Comparison of Crystallinity by SAXS and DSC. Figure 10 shows the ϕ_{PCL} dependence of linear crystallinity χ, defined by $\chi = l_c/(l_c + l_a)$ and evaluated from the curve fitting of the SAXS intensity with the H–T model, and bulk crystallinity χ' estimated from the DSC measurement. χ decreases as ϕ_{PCL} deviates from 1 and becomes invariant over the intermediate range of ϕ_{PCL}. It reflects the complicated change of l_a against ϕ_{PCL}, as shown in Figure 6b. χ increases with increasing T_c, mainly resulting from the fact that the lamella becomes thicker with increasing T_c (Figure 5a). χ' decreases linearly with decreasing ϕ_{PCL}, and the T_c dependence was negligibly small.

The difference in the ϕ_{PCL} dependence of χ and χ' can be qualitatively explained by taking account of the difference of the two methods employed for the crystallinity measurement. The SAXS intensity reflects only the structure within the crystalline domain and is intimately dependent on the values of l_c and l_a. This means that χ is independent of the existence of the amorphous domain outside the crystalline domain. The DSC thermogram, on the other hand, reflects the whole crystallinity of the system; the larger the portion of the amorphous (or PSO-rich) domain becomes, the smaller χ' is. Thus the large difference in the ϕ_{PCL} dependences of χ and χ', especially over the intermediate range of ϕ_{PCL}, indicates the complicated morphology formed by the combined effect of the crystallization of PCL and liquid–liquid phase separation in this PCL–PSO system.

Discussion

The SAXS curves obtained from the present PCL–PSO system consist of two components of the scattered intensity; one has a peak at ca. $s = 0.06$ nm^{-1} and arises from the crystalline domain consisting of alternating stacks of the lamellae and amorphous layers, and the other increases in intensity with decreasing s probably with the peak at $s = 0$ and arises from the average electron-density contrast between the crystalline and the amorphous domains (Figure 2). The SAXS curve shows that the second component of the scattered intensity grows steadily with decreasing ϕ_{PCL} (Figure 1), suggesting that the proportion of the amorphous domain increases with decreasing ϕ_{PCL}. The morphology formed in the system is strongly dependent on ϕ_{PCL} of the system; l_c is invariable against ϕ_{PCL} (Figure 5b), while l_a and N change significantly with ϕ_{PCL} (Figures 6b and 7b). The linear crystallinity, evaluated from l_c and l_a, depends strongly on ϕ_{PCL} in accordance with the ϕ_{PCL} dependence of l_a, while the bulk crystallinity measured by DSC linearly decreases with decreasing ϕ_{PCL} (Figure 10). The morphology formed in the system, on the other hand, is not so sensitive against T_c, though l_c and therefore the linear crystallinity increase linearly with increasing T_c.

The above results should be explained on the basis of the phase diagram of the present PCL–PSO system, where two phase transitions, binodals and crystallization of PCL, take place over the same temperature range. The typical phase diagram of such a system frequently appears in the fields of inorganic materials and alloys[22,23] and has recently been calculated in the field of polymer blends by Burghardt[7] on the basis of the Flory–Huggins type free energy. With the aid of the phase diagrams studied in such fields and thermodynamic principles, a schematic illustration of the phase diagram of the present system is constructed in Figure 11. Here L and C represent the disordered (amorphous) and ordered (perfect crystalline) phases, respectively. In the region denoted by $L_1 + L_2$, two disordered phases coexist, and in the region denoted by L + C, the disordered phase and perfect crystals of PCL coexist. At the temperature T_1, three phases, A, B, and C, coexist thermodynamically (eutectic temperature). It is important to note that the blend, quenched into the L + C region even if it is outside of the coexistence curve, always yields two phases; one is rich in PSO and the other consists of perfect crystals of PCL. In the case of the crystallization of polymers, the amorphous layer of PCL always exists between lamellae, and this layer can accommodate the PSO expelled from the lamella during the morphology formation to result in its composition variation. Therefore, it will be useful for better understanding to add the third phase M represented by a dashed curve in Figure 11, which represents the amorphous phase

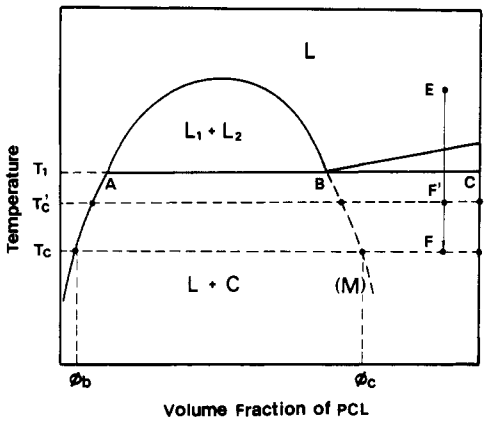

Figure 11. Speculative illustration of the phase diagram of the PCL–PSO system. L and C denote liquid and perfect crystalline phases, respectively, and the dashed curve represents the lower limit of ϕ_{PCL} in the amorphous layer between lamellae.

between lamellae and may be interpreted as a limit of the miscibility of PSO at the amorphous layer; the amorphous layer can accommodate PSO down to the composition represented by the dashed curve, but further increase of PSO results in phase separation in this layer. This third phase is not in thermodynamic equilibrium and may change in composition according to the thermodynamic and kinetic factors (or T_c and ϕ_{PCL}) in the process of morphology formation, but necessarily appears in the crystallization of polymers.

When a blend is quenched from the homogeneous state (E) into a two-phase region (F, $T = T_c$) denoted by L + C, the superstructure begins to appear in accordance with the reduction of free energy owing to the combined factor of crystallization and liquid–liquid phase separation. That is, the blend system has two phases in thermodynamic equilibrium: one is amorphous and rich in PSO and the other is pure PCL, and therefore the crystalline domain structure (alternating structure of lamella and amorphous layer) is favorable to reduce the free energy of the system. The amorphous component, PSO, rejected from the lamella during the crystallization process of PCL, is partly accommodated in the amorphous layer between lamellae. As a result, the blend has a morphology consisting of two domains; one is an amorphous domain having the composition of ϕ_b and the other is a crystalline domain made up of the lamella (perfect crystal) and amorphous layer with the PCL composition of ϕ_a ($\geq\phi_c$). At ϕ_{PCL} not far from 1, the ratio of the amorphous domain to the crystalline domain is too small to yield the X-ray intensity at smaller s scattered from the contrast between two domains. As ϕ_{PCL} decreases further, the proportion of the amorphous domain increases in the system, resulting in an increase of SAXS intensity at smaller s compared to the scattered intensity coming from the crystalline domain. Even if the blend is quenched to higher temperatures below the eutectic temperature (F', $T = T_c'$), the phase relation at T_c' is not largely different from that at T_c, so that the crystallization temperature does not significantly affect the morphology formed in the system and eventually does not affect the SAXS intensity. In the practical case, the kinetic factor intervenes into the process of the morphology formation within the system and may dramatically change the composition of the amorphous layer ϕ_a. In addition, at low crystallization temperatures, the mobility of the new amorphous domain is not enough to grow into a large domain and stay near the crystalline domain. At high crystallization temperatures, on the other hand, the mobility of the amorphous domain is sufficient that the domains may coagulate and grow larger. Thus, the kinetic factor may play an important role in the process of morphology formation in the PCL–PSO system. The microscopic observation by Tanaka and Nishi[14,15] in the PCL–PSO system, for example, clearly demonstrates the morphology difference when the blend is crystallized at different temperatures.

The validity of the above explanation should be confirmed by the quantitative comparison of the experimental data and the complete phase diagram of the system. The speculative discussion based on the tentative phase diagram, however, seems to be able to explain most of qualitative features observed in the SAXS and DSC measurements.

Acknowledgment. We thank the staff of the Workshop for Experimentation and Practice, School of Engineering, Nagoya University, for making sample holders to perform the SAXS experiment.

References and Notes

(1) Paul, D. R.; Newmann, S., Eds. *Polymer Blends*; Academic Press: New York, 1978; Vol. 1.
(2) Nose, T. *Phase Transitions* **1987**, *8*, 245.
(3) Hashimoto, T. *Phase Transitions* **1988**, *12*, 47.
(4) Stein, R. S.; Khambatta, F. B.; Warner, F. P.; Russell, T. P.; Escala, A.; Balizer, E. *J. Polym. Sci., Polym. Symp.* **1978**, *63*, 313.
(5) Endres, B.; Garbella, R. W.; Wendorff, J. H. *Colloid Polym. Sci.* *1985*, *263*, 361.
(6) Briber, R. M.; Khoury, F. *Polymer* **1987**, *28*, 38.
(7) Burghardt, W. R. *Macromolecules* **1989**, *22*, 2482.
(8) Inaba, N.; Sato, K.; Suzuki, S.; Hashimoto, T. *Macromolecules* **1986**, *19*, 1690.
(9) Inaba, N.; Yamada, T.; Suzuki, S.; Hashimoto, T. *Macromolecules* **1988**, *21*, 407.
(10) Hong, K. M.; Noolandi, J. *Macromolecules* **1983**, *16*, 1083.
(11) Roe, R. J.; Zin, W. C. *Macromolecules* **1984**, *17*, 189.
(12) Nojima, S.; Roe, R. J. *Macromolecules* **1987**, *20*, 1866.
(13) Nojima, S.; Terashima. Y.; Ashida, T. *Polymer* **1986**, *27*, 1007.
(14) Tanaka, H.; Nishi, T. *Phys. Rev. Lett.* **1985**, *55*, 1102.
(15) Tanaka, H.; Nishi, T. *Phys. Rev. A* **1989**, *39*, 783.
(16) Hosemann, R.; Bagchi, S. N. *Direct Analysis of Diffraction by Matter*; North-Holland: Amsterdam, 1962.
(17) Vonk, C. G.; Kortleve, G. *Kolloid Z. Z. Polym.* **1967**, *220*, 19.
(18) Glatter, O. *J. Appl. Crystallogr.* **1974**, *7*, 147.
(19) Porod, G. *Kolloid Z.* **1951**, *124*, 83.
(20) Tsvankin, D. *Polym. Sci. USSR (Engl. Transl.)* **1964**, *6*, 2304.
(21) Debye, P.; Bueche, A. M. *J. Appl. Phys.* **1949**, *20*, 518.
(22) Gordon, P. *Principles of Phase Diagrams in Materials System*; McGraw-Hill: New York, 1968.
(23) Christian, J. W. *The Theory of Transformation in Metals and Alloys*; Pergamon Press: Oxford, 1972.

Registry No. PCL (homopolymer), 24980-41-4; PCL (SRU), 25248-42-4; PSO (homopolymer), 9003-53-6.